# The October 27-28, 1986, FIRE Cirrus Case Study: Cloud Microstructure

Karen M. Miller
and
Andrew J. Heymsfield
National Center for Atmospheric Research[1]
Boulder, Colorado  80307

James D. Spinhirne
NASA Goddard Space Flight Center
Greenbelt, Maryland 20771

## 1. Introduction

Using aircraft in situ measurements, we examined the microphysics of cirrus clouds observed on 28 October 1986 during FIRE. We present our results as one component of an extensive coordinated study of the cirrus on this day. Our study contributes to the understanding of cold clouds by (i) providing microphysical data to supplement satellite and aircraft radiometer data for investigating cirrus cloud radiative effects; (ii) providing more complete information on ice particle evolution and cloud forcing mechanisms than was available in the past, through the use of instrumentation with higher resolution and more accurate calibration; (iii) expanding our knowledge of the particle characteristics in cold liquid water clouds, through improved instrumentation and by making use of sensors on other platforms, such as lidar; and (iv) by estimating the ice nucleus concentrations active at low temperatures in the upper troposphere from the concentrations of ice particles in colloidally stable liquid water clouds.

## 2. Aircraft instrumentation and flight locations

The clouds were sampled on 28 October 1986 in the vicinity of Green Bay and Wausau, WI. An upper level trough and a cold front from 400 mb to the surface were located in western Wisconsin. Details of the synoptic conditions are given by Starr and Wylie (1989).

The NCAR King Air turboprop and Sabreliner jet aircraft were used for the data collection. The period analyzed for the Sabreliner coincided with data collected from LANDSAT at 1553 UTC. The flight pattern included racetracks oriented about 30° off the mean horizontal wind direction of 260° at six altitudes from 8.6 to 11.3 km. The period analyzed for the King Air was just prior to and overlapped that for the Sabreliner. The flight pattern consisted of level traverses from 7.0 to 7.5 km.

Temperatures measured by the Rosemount sensors were accurate to ± 0.25°C, with a resolution of 0.006°C. Dew point temperatures were obtained from EG&G frost point hygrometers, which, at low temperatures, respond slowly and are of dubious accuracy. Liquid water (LW) was detected and the liquid water content (LWC) measured using Rosemount icing detectors (RICE). Droplet size spectra and the LWC were measured on the King Air using a Particle Measuring Systems (PMS) Forward Scattering Spectrometer Probe (FSSP) sizing from 1.5 to 46.5 $\mu m$ in 3 $\mu m$ bins beginning at 3 $\mu m$. Both aircraft were equipped with two PMS

357

2D probes to detect ice particles larger than 25–50 μm, but we will look at only the Sabreliner data here. Ice particle shapes (habits) and size spectra and estimated cloud ice water content (IWC) were derived from the 2D data and direct collections of particles on oil-coated slides.

## 3. Ice particle and droplet microphysics

Figure 1 depicts a vertical cross section of the attenuated backscatter observed by the ER-2 downward-looking lidar for 1552–1556 UTC as the aircraft overflew the study area. In the region shown, there are two cloud layers. The upper cirrus layer extends from 9.0 to 11.5 km. Much or all of the lower structure of this cirrus appears to result from precipitation of ice crystals from the thin layer above 11 km. The Sabreliner traverses were conducted within this higher cloud layer. The lower cloud layer from 7 to 8 km consists of two cloud types. A low density cirrus cloud is found between 15 and 25 km distance; this
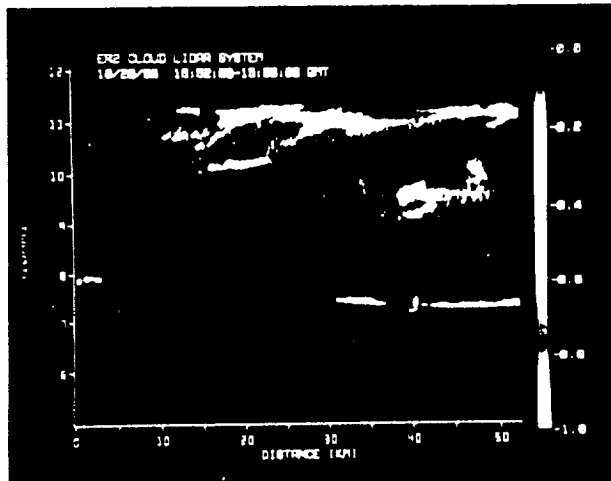
cloud, too, may result from precipitation of ice particles from about 8 km. An altostratus cloud less than 250 m thick is found elsewhere. Lidar depolarization data indicate that the altostratus layer was composed primarily of water droplets.

Ice particles >150 μm sampled by the Sabreliner probes at the upper cloud levels were primarily columns and compact spatial particles with extensions; those sampled at the lower levels were primarily bullet rosettes. Possibly this effect was due to the faster growth rate of the bullet rosettes or to the growth of compact spatial particles and/or additional nucleation in a convectively unstable layer between 9.50 and 9.65 km. Particles ≤150 μm were compact spatial particles, but we have little confidence in the habit assignment; these particles could have been plates or even columns.
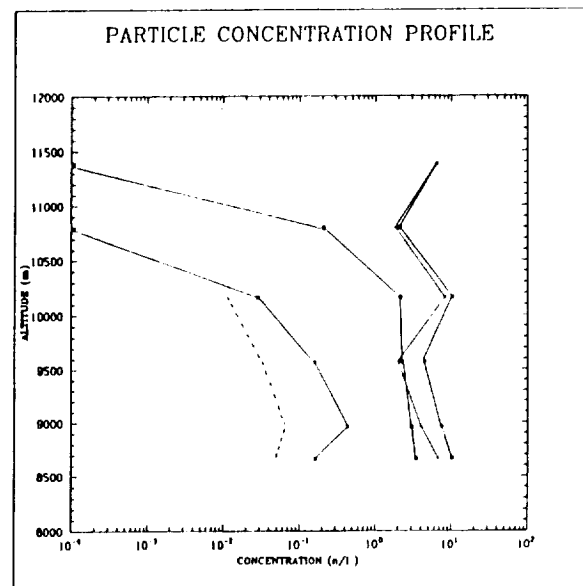


Figure 2. Ice particle concentration by size categories as a function of altitude (·: Total
[ ]: < 200 μm; ··: 200–500 μm; -: 500–... μm).

Figure 2 shows particle concentrations by size categories as a function of alti-



Figure 1. A vertical cross section of the attenuated backscatter observed by the ER-2 downward-looking lidar for 1552–1556 UTC as the aircraft overflew the study area.

tude. Concentrations decreased with increasing particle size, a spectrum typical of cirrus clouds. The total concentration was dominated by the concentration in the first size category. The concentrations in all size categories remained fairly constant with altitude; it is not known if this effect was due to particle fallout. But, notably, a sharp decrease in the concentrations of the larger particles occurred at the colder temperatures. The concentration of aggregates—particles containing two or more individual ice crystals—increased with decreasing altitude (Fig. 2, dashed line). Most of the large particles were aggregates.

The maximum ice particle dimension plotted in Fig. 3 shows a trend from smaller sizes at the cold temperatures near the cloud top to larger sizes at the base. The mass-weighted mean diameter shows a similar trend.
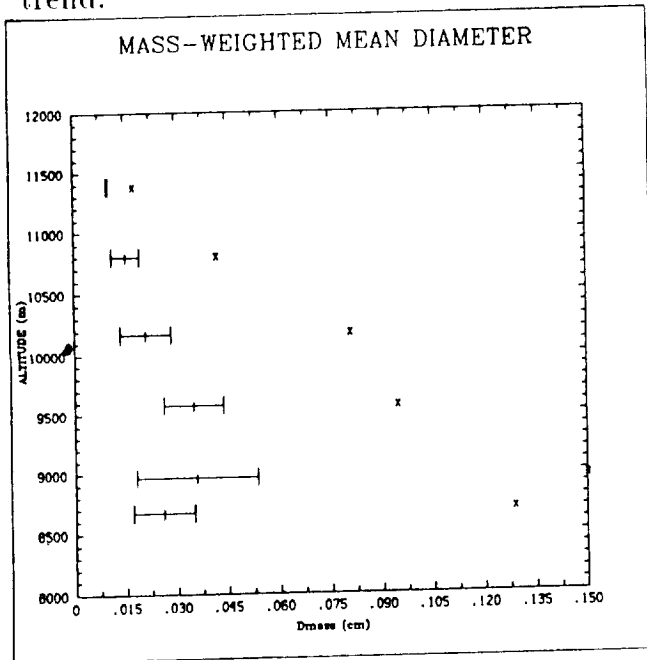


**Figure 3.** Maximum and mean mass-weighted ice particle dimensions as a function of altitude.

The IWC (Fig. 4) was calculated from the particle size spectra and habit percentages. The data show wide horizontal vari-

ability as indicated by the standard deviation about the mean. A dependence on north-south variability in the traverses is evident. Looking at the southern segments (traverses 1, 3, 5, from the top) and the northern segments (2, 4, 6) grouped separately, two distinct patterns of increasing IWC with decreasing altitude are seen; the value of IWC is consistently higher in the southern traverses.
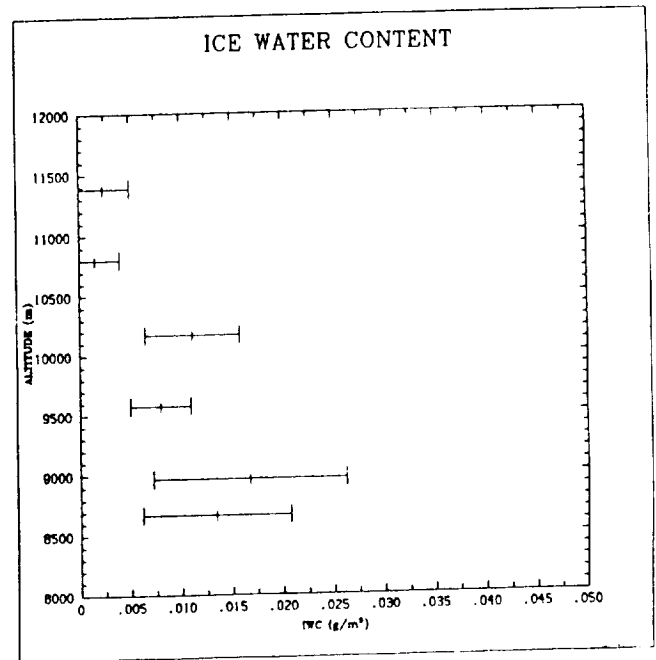


**Figure 4.** Ice water content as a function of altitude.

The cumulative distribution of ice mass as a function of altitude and particle size appears in Fig. 5. At the upper levels, the distribution indicates that considerable mass might be present below the minimum ice particle size detectable with the 2D-C probe. At the lower levels, probably most of the ice mass is detectable.

Liquid water was measured from the King Air in ten separate events at altitudes ranging from 7.30 to 7.15 km and spanning a horizontal distance of 0.5 to 7.0 km. An event was a period of continuous LW detection, that is, where no more than one consecutive second elapsed without LW detection.

The LWC averaged over each traverse was typically less than 0.005 g m$^{-3}$. Droplet concentrations were less than 70 cm$^{-3}$, and average diameters were smaller than 7 μm. Ice particle concentrations in these events were extremely low, less than 0.05 ℓ$^{-1}$.

Figure 6 shows a high resolution view of the lidar backscatter within the altocumulus layer. The mean droplet diameters and the LWC observed from the King Air during an ascent through this layer are shown in Figs. 7A and 7B. The scale of horizontal variability in LWC is commensurate with the scale of changes in lidar backscatter, approximately 0.5 km. The LWC was about half the adiabatic value, and since ice mass was negligible within the layer, mixing was evidently reducing the LWC. From the temperature data, we concluded that the cloud was convectively stable, and that the cloud layer lifted from above an inversion at the base of the LW region.

## 4. Conclusions

We examined the microstructure of the ice and liquid water phases for the FIRE cirrus case study of 28 October, 1988, using measurements taken from two aircraft between 6 and 12 km. We characterized ice particle and droplet concentrations, and ice and liquid water contents.

Our data indicate that the cirrus resulted from weak uplift of 10 cm s$^{-1}$ or less and the LW layer sampled at the satellite overpass time resulted from forced ascent at 25 cm s$^{-1}$ above a sloped temperature inversion. The LW layer was capped by a stable layer; calculated Richardson numbers were < 0.25, suggesting that this zone may have contained Kelvin-Helmholz waves.

The most significant microphysical finding was the persistence of liquid water clouds at temperatures about −30°C. Virtually no ice particles were detected in the cloud. Also of importance was the observation of ice crystal aggregates at temperatures as low as −56°C. Aggregation accounted for the development of most of the larger particles present, since the growth rates of aggregates are much higher than the rates for single crystals.

## REFERENCES

Starr, D. O'C., and D. P. Wylie, 1989: The October 27–28, 1986, FIRE cirrus case study: Meteorology and cloud fields. *Mon. Wea. Rev.* (in submission).
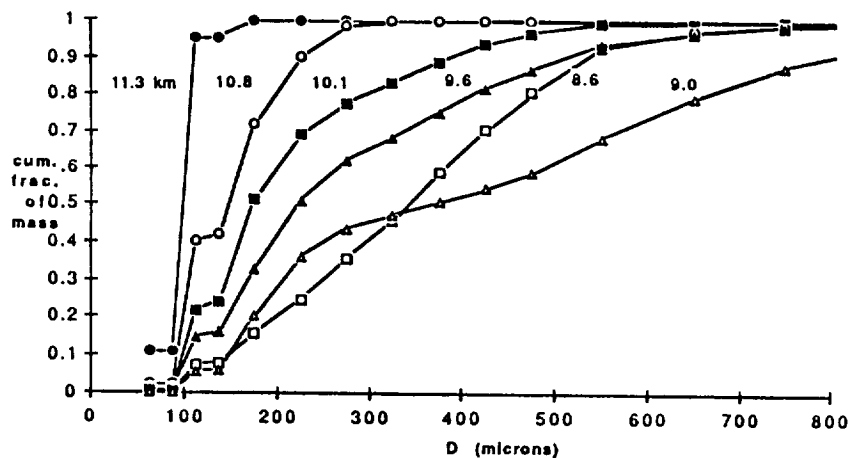


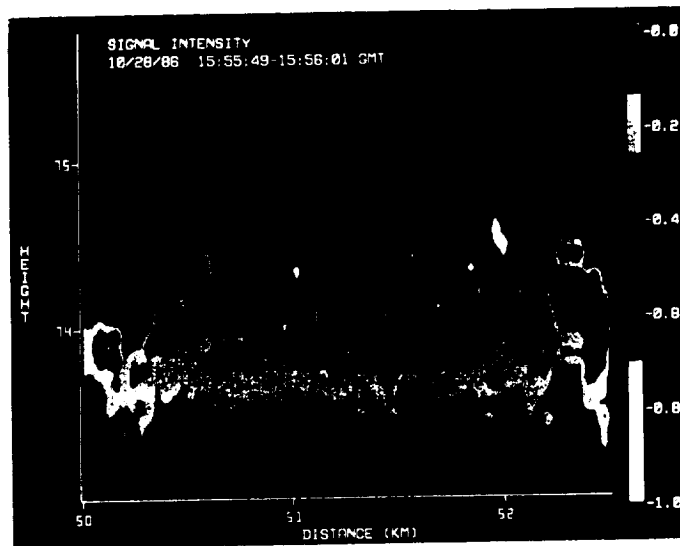Figure 5. Cumulative distribution of ice mass as a function of altitude and particle size.

**Figure 6.** Lidar backscatter cross section observed by ER-2 lidar 1552 1556 UTC, showing altocumulus layer sampled by King Air. (Height is km × 10.)
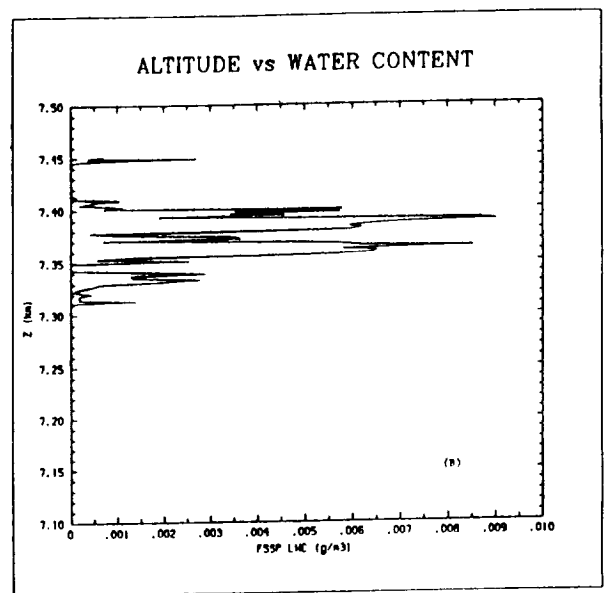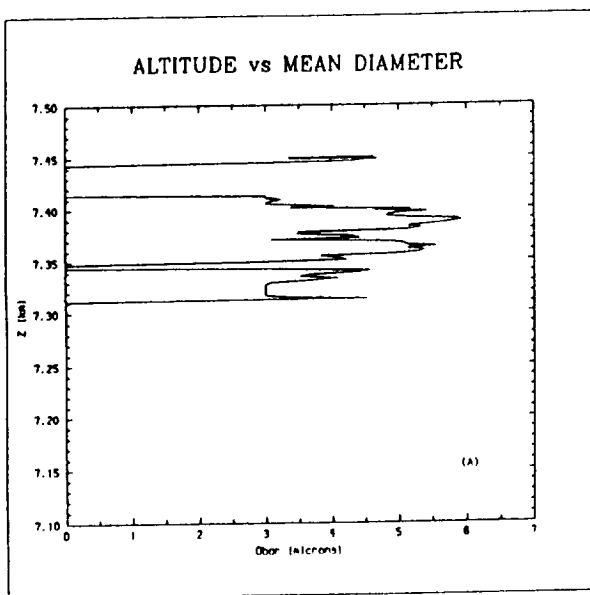


**Figure 7.** Data in LW region during King Air ascent 152545–152820 UTC. Panel A: Mean droplet diameter. Panel B: Liquid water content.